



HAL
open science

Efficient conversion of hemicellulose into high-value product and electric power by enzyme-engineered bacterial consortia

Bo Liang, Jing Yang, Chen-Fei Meng, Ya-Ru Zhang, Lu Wang, Li Zhang, Jia Liu, Zhen-Chao Li, Serge Cosnier, Ai-Hua Liu, et al.

► **To cite this version:**

Bo Liang, Jing Yang, Chen-Fei Meng, Ya-Ru Zhang, Lu Wang, et al.. Efficient conversion of hemicellulose into high-value product and electric power by enzyme-engineered bacterial consortia. *Nature Communications*, 2024, 15 (1), pp.8764. 10.1038/s41467-024-53129-0 . hal-04744227

HAL Id: hal-04744227

<https://hal.univ-grenoble-alpes.fr/hal-04744227v1>

Submitted on 18 Oct 2024

HAL is a multi-disciplinary open access archive for the deposit and dissemination of scientific research documents, whether they are published or not. The documents may come from teaching and research institutions in France or abroad, or from public or private research centers.

L'archive ouverte pluridisciplinaire **HAL**, est destinée au dépôt et à la diffusion de documents scientifiques de niveau recherche, publiés ou non, émanant des établissements d'enseignement et de recherche français ou étrangers, des laboratoires publics ou privés.

1 **Efficient conversion of hemicellulose into high-value product and electric power by**
2 **enzyme-engineered bacterial consortia**

3 Bo Liang¹, Jing Yang¹, Chen-Fei Meng¹, Ya-Ru Zhang², Lu Wang¹, Li Zhang¹, Jia Liu¹,
4 Zhen-Chao Li², Serge Cosnier^{3,4,5*}, Ai-Hua Liu^{2*}, and Jian-Ming Yang^{1*}

5

6 ¹Energy-rich Compounds Production by Photosynthetic Carbon Fixation Research Center,
7 Shandong Key Lab of Applied Mycology, College of Life Sciences, Qingdao Agricultural
8 University, Qingdao 266109, China.

9 ²Institute for Chemical Biology & Biosensing, and College of Life Sciences, Qingdao
10 University, Qingdao 266071, China.

11 ³Centre for Organic and Nanohybrid Electronics, Silesian University of Technology,
12 Konarskiego 22B, 44-100 Gliwice, Poland

13 ⁴Department of Physical Chemistry and Technology of Polymers, Silesian University of
14 Technology, M. Strzody 9, 44-100 Gliwice, Poland

15 ⁵DCM UMR 5250, Université Grenoble-Alpes, F-38000 Grenoble, France; Departement de
16 Chimie Moléculaire, UMR CNRS, DCM UMR 5250, F-38000 Grenoble, France.

17 *Correspondence: serge.cosnier@univ-grenoble-alpes.fr

18 liuah@qdu.edu.cn

19 yjming888@126.com

20

21

22

23 **Abstract:**

24 As an abundant agricultural and forestry biomass resource, hemicelluloses are hard to be
25 effectively degraded and utilized by microorganisms due to the constraints of membrane and
26 metabolic regulations. Herein, we report a synthetic extracellular metabolic pathway with
27 hemicellulose-degrading-enzymes controllably displayed on *Escherichia coli* surface as
28 engineered bacterial consortia members for efficient utilization of xylan, the most abundant
29 component in hemicellulose. Further, we develop a hemicellulose/O₂ microbial fuel cell
30 (MFC) configuring of enzyme-engineered bacterial consortia based bioanode and
31 bacterial-displayed laccase based biocathode. The optimized MFC exhibited an open-circuit
32 voltage of 0.71 V and a maximum power density (P_{max}) of $174.33 \pm 4.56 \mu\text{W cm}^{-2}$.
33 Meanwhile, 46.6% (w/w) α -ketoglutarate was produced in this hemicellulose fed-MFC.
34 Besides, the MFC retained over 95% of the P_{max} during 6 days' operation. Therefore, this
35 work establishes an effective and sustainable one-pot process for catalyzing renewable
36 biomass into high-value product and powerful electricity in an environmentally-friendly way.

37

38

39

40

41

42

43

44

45 **Introduction**

46 Lignocellulose, which is produced through photosynthesis by plant, is a huge solar energy
47 reservoir. As a green and sustainable alternative to fossil energy, it has attracted a broad
48 interest to explore lignocellulose biomass for high added-value products and biofuel^{1, 2}.
49 Biological hydrolysis and fermentation process of lignocellulosic biorefinery are regarded as
50 the most promise and eco-friendly approach compared to physical and chemical methods^{3, 4}.
51 As the most abundant component in lignocellulose, cellulose can be easily metabolized by
52 most microorganism owing to only glucose units⁵. Whereas, hemicellulose, accounting for
53 20-40% of lignocellulose, are hard to be effectively degraded and utilized by many
54 microorganisms due to the heterogeneous structure of hemicellulose and the constraints of
55 effective membrane transporters as well as the metabolic regulations *in vivo*^{6, 7}. Thus, the low
56 utilization efficiency of hemicellulose greatly affect lignocellulosic biorefinery⁸.

57 Currently, hemicelluloses have been used to produce valuable chemicals such as ethanol,
58 furfural and xylitol⁹. Unfortunately, these processes still experience challenges of low
59 conversion activity and poor stability of cells. For example, the yield of
60 hemicelluloses-bioethanol is lower than that of bioethanol fermented from cellulose owing to
61 the poor utilization efficiency of polysaccharide and pentose by microorganisms during
62 fermentations¹⁰. Besides, bioelectric energy has been heralded as a one of the most potential
63 renewable energies in the future^{11, 12}. To realize the generation of energy from hemicelluloses
64 biomass, great efforts via recruitment of microbial community (microbial fuel cells, MFCs)
65 have been devoted¹³. However, diverse biological properties in one system result in the
66 instability in bacterial community, which severely limits its large-scale application¹⁴. To

67 address these challenges, a strategy is highly desirable to realize high-efficient production of
68 biofuels and biochemicals directly from hemicellulose instead of its monosaccharides.

69 As an efficient and green method, enzymatic catalysis has been employed to hydrolyze
70 polysaccharides and oxidize monosaccharides. However, the high-cost and poor stability
71 greatly limit their large-scale applications¹⁵. Meanwhile, microbial fermentation is another
72 main biological approach to produce biofuels and biochemicals. The cell membrane barrier
73 and intracellular metabolic regulation always restrict the highly efficient substrate utilization,
74 especially polysaccharides¹⁶. Enzymes can be displayed on microbial surface and the resulted
75 whole-cell biocatalyst was obtained by large-scale fermentation and directly applied in
76 biocatalytic reactions without tedious protein purification process, which enables to
77 implement complex biochemical reactions even metabolic pathways without the constraints
78 of cell membrane and metabolic regulation^{17, 18, 19}. Similar with secreted proteins, displayed
79 enzymes could be expressed and folded in periplasm and exported directly across cell membrane
80 of *E. coli* to the culture medium using Sec secretory system²⁰. The displayed enzymes could be
81 assembled and anchored onto outer membrane by fusing with anchoring motif, which could
82 facilitate their abilities to be recycled and regenerated. In contrast, secreted proteins will be folded
83 in cytoplasm or periplasm, depending on the sec or tat signal sequence used, and then secreted and
84 dispersed in the culture media without geographical restrictions of cell surface, failing to be
85 recycled or regenerated²¹.

86 Herein, we report on an artificial hemicellulose degrading pathway catalyzed by the
87 engineered bacterial consortia whose enzymes from various origins are recruited to achieve
88 the optimal overall reaction rate in a controlled manner, for the high-efficiently converting

89 renewable biomass into electric energy and high-value chemical simultaneously in an
90 environmentally-friendly way. The engineered *Escherichia coli* (*E. coli*) (up-stream pathway
91 members) degrade xylan, the most abundant biopolymer in hemicellulose²², into
92 monosaccharides, while the following recombinant *E. coli* (down-stream pathway members)
93 oxidize monosaccharides into α -ketoglutarate accompanied by generating the reduced form of
94 nicotinamide adenine dinucleotide (NADH) (Fig. 1). Thus *denovo* MFC is designed to
95 achieve one-pot efficient production of high added-value chemical of α -ketoglutarate and
96 powerful electricity from hemicellulose biomass in a “one-stone-two-birds” manner,
97 demonstrating a model to efficiently utilize biomass in a sustainable way.

98

99 **Results and discussion**

100 **Bacterial surface displaying enzymes (engineered bacterial consortia) involving in the** 101 **saccharification of xylan (up-stream pathway)**

102 Herein, the utilization of xylan experienced two stages, firstly saccharified into
103 monosaccharides (mainly D-xylose), which are then oxidized to produce α -ketoglutarate and
104 release electrons. For the initial phase, hemicellulases hydrolyze β -linkage in the xylan
105 backbone to release monosaccharides. A marine symbiont *Teredinibacter turnerae* was
106 selected as the bacterial endo- β -1,4 xylanases (TtGH8) source. TtGH8 shows a wide variety
107 of glycoside hydrolases activities including β -1,4 xylanases, especially the highest activity on
108 mixed-linkage β -1,3 and β -1,4 xylanases²³, which could expand the panel of substrate used in
109 our system. β -D-xylosidase (SXA) from *Selenominas ruminantium* exhibits good
110 thermo-stability as well as superior activity towards 1,4- β -D-xylooligosaccharides^{24, 25}.
111 Besides, SXA also has α -arabinofuranosidase activity towards arabino xylanases²⁶. The

112 synergy of these two hemicellulases could break down xylan into monosaccharides.
113 Unfortunately, *E. coli* BL21 (DE3) can metabolize xylose under the action of xylose
114 isomerase (XylA) and xylulose kinase (XylB)²⁷. Therefore, in order to drive all of the
115 generated xylose by hemicellulase into the designed extracellular metabolic pathway and
116 avoid monosaccharides waste, *xylA* and *xylB* genes in *E. coli* BL21 (DE3) were knocked out.

117 During the first stage, when applying two types of hydrolase-displaying on the surface of
118 bacterial cell, polysaccharide generated from lignocellulose pretreatment could be
119 immediately degraded into monosaccharide by these displayed enzymes in a high efficient
120 way without passing through cell membrane²⁸. TtGH8 and SXA were displayed on cell
121 surface separately or simultaneously as fusion protein using N-terminal region of ice nuclear
122 protein from *P. borealis* (InaPb) as anchoring motif²⁹. The connection manner of cell surface
123 displayed TtGH8-SXA was optimized by introducing linkers Gly-Ser,
124 Gly-Ser-Gly-Gly-Ser-Gly and (Ala-Pro)₇ between TtGH8 and SXA, respectively. Results
125 show that the engineered strains harboring GS and GSGGSG linkers had similar activities.
126 However, (AP)₇ linker influenced the functions of cell surface displayed TtGH8-SXA, and the
127 whole-cell activity reduced 50% compared to that of strain displayed TtGH8-SXA with GS
128 linker. Therefore, Gly-Ser was employed as the linker between TtGH8 and SXA. Surface
129 displaying-enzymes demonstrated obvious expression levels, which were confirmed by
130 Western Blotting (Supplementary Fig. 1) and confocal imaging (Supplementary Fig. 2). Next,
131 biochemical activity assays were conducted to validate biological functions of
132 surface-displayed enzymes by using commercial xylan as substrate using 3,5-dinitrosalicylic
133 acid (DNS) method. The optimized protein expression conditions for displayed enzymes were

134 0.5 mM isopropyl- β -D-thiogalactopyranoside (IPTG) and 30 °C (Supplementary Fig. 3).
135 However, when IPTG concentration was over 1.0 mM, the whole-cell activities of engineered
136 strains were declined due to the imbalance of transcription and secretion³⁰. According to
137 results of Quantitative Immunoassay (Supplementary Fig. 4), the number of cell surface
138 displayed proteins were estimated. Strains displayed different amounts of these enzymes,
139 approximately 25560, 25300 and 18020 enzyme molecules for TtGH8, SXA and TtGH8-SXA,
140 respectively. The fewer number of TtGH8-SXA displayed on the surface of per cell suggests
141 the decreased display efficiency for protein with a larger molecule (108 kDa). On the basis of
142 the number of enzymes displayed on cell surface, the effects of single display system and
143 dual-display system on saccharification of hemicellulose were investigated. As can be seen
144 from Supplementary Fig. 5, the strain displaying fusion protein TtGH8-SXA exhibited a
145 30.37% lower activity towards xylan than the mixture of two strains displaying TtGH8 and
146 SXA individually with molar ratio of 1:1 at the same levels of displayed enzyme molecules,
147 probably due to the lower protein numbers of TtGH8-SXA on cell surface compared to the
148 sum of TtGH8 and SXA single-displayed numbers. Then, the ratio of cell density of two
149 engineered strains was optimized to efficiently hydrolyze xylan into monosaccharides. As
150 indicated in Fig. 2a, different ratios of strain *E. coli*-TtGH8 to *E. coli*-SXA resulted in
151 different hydrolysis efficiency with the best ratio of 3:7. TtGH8 and SXA possess different
152 functions during the degradation process of xylan. TtGH8 is responsible for degrading xylan
153 into xylooligosaccharide as well as a small amount of D-xylose and L-arabinose²³. The
154 xylooligosaccharide could be further hydrolyzed into D-xylose and L-arabinose under the
155 action of SXA. So, the amounts of required SXA were higher than those of TtGH8 for full

156 hydrolyzation of xylan into monosaccharides. The hydrolysis efficiency of up-stream
157 bacterial consortia including *E. coli*-TtGH8 and *E. coli*-SXA towards xylan at different
158 concentrations were examined. To quantify the proportion and amounts of pentose in the
159 hydrolysate after strains' treatment, the resultant D-xylose and L-arabinose were determined
160 by HPLC method, accounting for 97.43% and 2.57%, respectively. Although the efficiency of
161 saccharification was increased with the decreasing xylan concentration from 1 g/L to 0.1 g/L,
162 the yields of pentose monomers also reduced accordingly (Supplementary Fig. 6). When
163 corncob xylan was 1 g/L, the hydrolysis efficiency was 65.43% (w/w) after 6 h reaction
164 (Supplementary Fig. 6), which was about 1.42-fold higher than *in vitro* process³¹ and
165 1.65-fold higher than *in vivo* process reported previously³². When the concentration of xylan
166 continued to increase, the production of pentose failed to rise proportionally. Anyway, this
167 simple bacterial consortium could generate soluble monosaccharides from xylan ready for the
168 subsequent oxidative degradation.

169

170 **Engineered bacterial consortia involving in oxidation of pentose monosaccharides** 171 **(down-stream pathway)**

172 To date, D-xylose metabolism pathway has been found in a few microorganisms, which
173 harbors three catabolic routes, including the Weimberg or Dahms pathway, the
174 xylulose-1-phosphate or ribulose-1-phosphate pathway and the xylose isomerase or xylose
175 reductase-xylylitol dehydrogenase pathway³³. *E. coli* can utilize xylose as a carbon source for
176 growth through the native route mediated by XylA and XylB as well as pentose phosphate
177 pathway and the glycolysis. However, the low efficiency limited the application of this
178 pathway in metabolic engineering³⁴. Weimberg route in *Caulobacter crescentus* involves

179 conversion of D-xylose to α -ketoglutarate by five steps successively catalyzed by XDH, XylC,
180 XylD, XylX and KGSADH³⁵ (Fig. 1). This pathway has been proved to be an attractive route
181 for biosynthesis of various chemicals from xylose^{34, 36, 37}. In our current study, the oxidation of
182 pentose and the transferring of electrons could be realized by employing this efficient
183 pathway, during which 1 molecule of α -ketoglutarate and 4 electrons per pentose unit can be
184 generated.

185 To identify the biological activity of each enzyme involved in Weimberg pathway, the *in*
186 *vitro* activities of the purified enzymes were measured. Proteins expression conditions were
187 optimized (Supplementary Fig. 7) and enzymes were purified to homogeneity through Ni²⁺
188 column affinity chromatography before SDS-PAGE analysis (Supplementary Fig. 8). In this
189 first step of Weimberg pathway, D-xylose is oxidized into D-xylono-lactone and generates
190 NADH catalyzed by XDH using NAD⁺ as coenzyme. So, the activity of XDH was monitored
191 by measuring the absorbance at 340 nm, typical absorption peak of NADH. As listed in
192 Supplementary Table 3, the enzymatic activity of XDH was 1195.00 ± 8.60 U/mg. To
193 examine the activity of XylC, D-xylono-lactone was used as substrate to produce D-xylonic
194 acid. The enzymatic activity of XylC was 146.93 ± 2.16 U/mg, which was 7-fold lower than
195 that of XDH (Supplementary Table 3). Subsequently, D-xylonic acid would be transformed
196 into 2-keto-3-deoxyxylic acid by XylD with an activity of 77.00 ± 3.00 U/mg. The activity of
197 KGSADH is 54.00 ± 6.00 U/mg, which was also monitored by measuring the generation of
198 NADH using analogous glutaraldehyde as substrate. Finally, the enzymatic activity of XylX
199 was determined only 35.65 ± 0.25 U/mg (Supplementary Table 3) by a coupled assay with
200 XylD and KGSADH. Thus XylX possessed the lowest activity among these five enzymes

201 involved in Weimberg pathway. Therefore, all of the enzymes had biological functions, but
202 the conversion of 2-keto-3-deoxyxylic acid to 2,5-dioxopentanoate catalyzed by XylX may be
203 a limiting step in the overall route, as proposed in other literatures³⁷.

204 On the basis of the *in vitro* analysis of these five members in Weimberg pathway,
205 cell-surface display systems were constructed. To confirm that the localization of enzymes on
206 the surface of *E. coli* using InaPb anchoring motifs, Western-Blot analysis of outer membrane
207 fraction and immunofluorescent labeling of cells were conducted. All the distinct bands of
208 expected sizes from outer membrane fractions were found (Supplementary Fig. 9), confirming
209 that the introduced genes in different recombinant plasmids were expressed obviously.
210 Compared with the control strain, green fluorescence was visualized for strains samples by
211 confocal microscope (Supplementary Fig. 10). To ascertain the displayed enzymes possessed
212 functions on the surface of bacteria, the whole-cell was regarded as the catalyst in the
213 enzymatic activity assay. After optimizing the protein expression conditions for displayed
214 enzymes (Supplementary Fig. 11), the whole-cell activities were determined. As depicted in
215 Tables S3 and S4, XDH-displaying *E. coli* exhibits the highest activity of 1.25 ± 0.04 U/OD₆₀₀
216 with k_{cat} value of 11.34 ± 1.21 s⁻¹. The whole cell activity of *E. coli*-XylC was significantly
217 lower than that of *E. coli*-XDH. So, the co-display of XDH and XylC would lead to the
218 imbalance of cascade reaction. Therefore, the maximum cascade reaction rate could be
219 achieved by separately displaying XDH and XylC on cell surface and regulating the ratio of
220 strain *E. coli*-XDH and *E. coli*-XylC. On the contrary, XylX-displaying *E. coli* shows the
221 lowest activity (0.044 ± 0.003 U/OD₆₀₀) with k_{cat} value of 0.07 ± 0.006 s⁻¹, which corresponds
222 to the *in vitro* data. These results reveal that XylX was the rate-limiting enzyme in the whole

223 pathway, so the highest overall reaction rate could be realized by adjusting the level of *E.*
224 *coli*-XylX in engineered bacterial consortia.

225 Considering the imbalance of activities between *E. coli* displaying enzymes, the
226 dual-display and tri-display systems were developed to accelerate the overall reaction rate of
227 the latter half of the pathway. The Western Blotting analysis and confocal imaging
228 micrographs indicate the successful expression and display of fusion enzymes on cell surface
229 (Supplementary Fig. 9 and Supplementary Fig. 10). Unfortunately, the degradation of triple
230 fusion protein XylX-XylD-KGSADH was observed, implying the unstable presentation of
231 much larger protein (157 kDa) on cell surface. The overall reaction rates from D-xylonic acid
232 to α -ketoglutarate were varied using different display systems as biocatalysts. Among them,
233 the bacterial consortia containing XylD-KGSADH-displaying *E. coli* (*E. coli*-XylDK) and
234 XylX-displaying *E. coli* (*E. coli*-XylX) exhibited the best catalytic efficiency when using
235 D-xylonic acid as substrate and NADH as indicator (Fig. 2b). Then, the cell density ratios of
236 down-stream pathway were optimized to realize the maximum overall reaction rate from
237 D-xylonic acid to α -ketoglutarate. Considering the highest activity of *E. coli*-XDH in the five
238 whole-cell catalysts, the ratio of *E. coli*-XDH in the prepared bacterial consortia was
239 controlled at a lower level. The ratios of other three strains, including *E. coli*-XylC, *E.*
240 *coli*-XylDK and *E. coli*-XylX, were varied to realize the highest overall reaction rate from
241 D-xylonic acid to α -ketoglutarate. As shown in Fig. 2c, the ratios of *E. coli*-XylDK and *E.*
242 *coli*-XylX had obvious synergistic effect on the generation of the final product α -ketoglutarate.
243 Thus, the Weimberg pathway can function in the engineered bacterial consortia.

244
245

246 **The integration of the engineered bacterial consortia for producing α -ketoglutarate**

247 To integrate the entire pathway for degrading xylan, according to above optimized
248 enzyme-displaying strain ratios in up-stream pathway and down-stream pathway, these
249 involved enzyme-displaying strains were mixed into bacterial consortia with different ratios
250 of cell densities in the saccharification of xylan into pentose and the oxidation pentose into
251 α -ketoglutarate. The most appropriate ratio was 3:7 for bacterial consortia in up-stream route
252 to down-stream route with the total OD₆₀₀ of 10.0 taking the titer of α -ketoglutarate as
253 evaluation criterion (Fig. 2d). These results demonstrate that the imbalanced enzymes
254 activities could be adjusted by optimizing strain ratios.

255 α -Ketoglutarate is not only an important intermediate metabolite in cells, but also is
256 widely used as antioxidant and nutrient supplements in food and pharmaceutical fields³⁸. Due
257 to the low efficiency and complex process of chemical synthetic route³⁹, α -ketoglutarate is 10
258 times more expensive than other common organic acids such as citric acid and lactic acid.
259 Moreover, the usage of toxic chemical reagent cyanide in chemical reaction process has
260 aroused the concerns of environmental pollution. The microbial synthesis method is
261 characterized as cost-effective, high efficient and eco-friendly⁴⁰. Until now, *Yarrowia*
262 *lipolytica* and *Corynebacterium glutamicum* have been engineered as microbial cell factories
263 to produce α -ketoglutarate using various substrates, such as raw glycerol and xylose (Table 1).
264 Compared with these substrates, hemicellulose is considered to be the most promising
265 feedstock due to its global availability and cost-effective benefits. Herein, to the best of our
266 knowledge, the employment of renewable hemicellulose to produce α -ketoglutarate was
267 realized for the first time with the yield of 47% (g/g) within 6 h *in vitro* one-pot reaction by

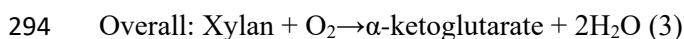
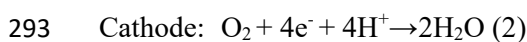
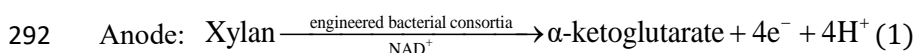
268 the engineered bacterial consortia saccharification and oxidation pathway. Our yield reaches
269 the highest level within 6 h, which is significantly shorter than over 90 h for microbial cell
270 factories using cost-ineffective glycerol and xylose as substrates (Table 1). It is worth noting
271 that, as the pivot metabolites among tricarboxylic acid cycle (TCA cycle), glyoxylate cycle
272 and amino acid metabolism, the generation of α -ketoglutarate would be impacted by complex
273 metabolic regulation *in vivo*. In this study, extracellular pathway circumvented this bottleneck
274 and improved the synthetic efficiency. Thus, the bioproduction of α -ketoglutarate from
275 hemicellulose in this work realized the efficient conversion of agricultural and forestry
276 residues to high-added value compound.

277

278 **The integration of the engineered bacterial consortia for generating electricity in MFC**

279 Fig. 3 describes the mechanism of the two-compartment xylan/O₂ MFC separated by a
280 Nafion® membrane. The mediator-less anodic compartment containing multi-walled carbon
281 nanotubes (MWCNTs) covered carbon cloth (CC) electrode, which was modified with
282 engineered bacterial consortia (CC/MWCNTs/bacterial-consortia) and fuel of xylan, while the
283 cathodic compartment contained MWCNTs-coated CC electrode, which was modified with *E.*
284 *coli*-displayed laccase (Lac) (CC/MWCNTs/*E.coli*-Lac) and 2,2'-azino-bis
285 (3-ethylbenzothiazoline-6-sulfonic acid) (ABTS) as the redox mediator. Lac was confirmed to
286 display on the cell surface by SDS-PAGE, Western-Blot and confocal imaging
287 (Supplementary Fig. 12) with good catalytic activity (Supplementary Fig. 13), which
288 catalyzes the O₂ reduction at the cathode (Fig. 4a). *E.coli*-Lac exhibits the maximum activity
289 at pH 5.0 (Supplementary Fig. 13c). The synthetic metabolic pathway on the anode

290 compartment was designed to degrade xylan into α -ketoglutarate, generating 4 electrons per
291 pentose unit. The reactions can be expressed as:



295 The performance of the biocathode and bioanode was examined by Cyclic voltammetry
296 (CV). At the CC/MWCNTs/*E.coli*-Lac, ABTS exhibited a redox pair in the absence of oxygen
297 (red line), while the cathodic specific current significantly enhanced in the presence of O_2
298 (Fig. 4a, light blue line), indicating that with ABTS as the electron transfer mediator, the
299 bacteria-displayed laccase catalyzes the reduction of oxygen. For bioanode, as shown in Fig.
300 4b, an onset potential at 0.13 V (vs. Ag/AgCl) for enzyme-displayed *E. coli* was observed (red
301 line). Interestingly, the onset potential for CC/MWCNTs/bacterial-consortia was negatively
302 shifted to 0 V (blue line), suggesting that the generated NADH from NAD^+ was catalytically
303 oxidized by MWCNTs⁴³. 9,10-anthraquinone-2,7-disulfonic acid (AQDS) was used as
304 electron mediator to investigate the impact of electron transfer mechanisms on the
305 performance of bioanode. As shown in Fig. 4b, the two reduction peaks (green curves) at -0.6
306 V and -0.9 V were the reduction peaks of AQDS with MWCNTs modified CC as electrode.
307 The oxidation peak of AQDS was around -0.5 V on the purple curve, which was shifted to
308 around -0.4 V due to the influence of CC modified with bacterial consortia. The oxidizing
309 redox peak around -0.1 V on the purple curve was the oxidation peak of NADH produced by
310 the catalysis of bacterial consortia in the presence of AQDS. AQDS can lower the onset
311 potential of NADH which was produced by cell-surface displayed enzymes' catalysis. The
312 onset potential was negatively shifted to -0.20 V (purple line). Therefore, this mediator was

313 implemented in the electrolyte of anodic chamber in the following studies.

314 Then, we studied the performance of MFCs composed of the above prepared bioanode
315 and biocathode by varying the way of loading engineered strains. The current density (j_{\max}) of
316 the generated MFC was $371.67 \pm 10.36 \mu\text{A}\cdot\text{cm}^{-2}$ when bacterial consortia were immobilized
317 on electrode (Fig. 4c, light green line). However, the j_{\max} of MFC dropped to 297.54 ± 10.24
318 $\mu\text{A}\cdot\text{cm}^{-2}$ when bacterial consortia were dispersed in bioanode chamber (Fig. 4c, blue line).
319 Then the effects of different concentrations of AQDS on the performance of xylan/O₂ MFC
320 were investigated. The results show that the highest value of power was achieved when 10
321 mM of AQDS was used (Fig. 4c, peach pink line). The similar trends were observed in Fig.
322 4d, and the constructed MFC reached the maximum power output (P_{\max}) of 68.25 ± 2.38
323 $\mu\text{W}\cdot\text{cm}^{-2}$ when bacterial consortia immobilized on bioanode in the presence of 10 mM of
324 mediator AQDS.

325 *Shewanella oneidensis* is one of the most well-known electricigen in nature⁴⁴. The
326 attempt to engineer *S. oneidensis* MR-1 using D-xylose as fuel to generate bioelectricity in
327 MFC by introducing D-xylose metabolic route shows restricted power owing to poor
328 efficiency of this exogenous pathway⁴⁵. Herein, we reconstituted a D-xylose oxidative
329 pathway and electron transfer chain on cell surface by displaying Weimberg pathway
330 members. There are two steps can produce NADH for generating power, which were
331 catalyzed by XDH and KGSADH. Finally, the oxidation of one D-xylose can yield two
332 NADH and four electrons during the whole process, and the final metabolite α -ketoglutarate
333 can be used as the key precursor of several medicine and nutrient substance in food as well as
334 feed⁴⁶.

335 **The optimization of MFC performance**

336 To boost the power output of MFC, effects of several parameters on electricity generation
337 were investigated. First, the loading amounts of bacterial consortia on the bioanode was
338 optimized. The j_{\max} of MFCs was $671.33 \pm 26.21 \mu\text{A}\cdot\text{cm}^{-2}$, corresponding P_{\max} of $112.87 \pm$
339 $7.83 \mu\text{W}\cdot\text{cm}^{-2}$ when loading 10 OD₆₀₀ bacterial consortia (Fig. 5a, peach pink line). The
340 results indicate that the bacterial cell loading exerted effects on power output since the
341 insulated nature of concentrated cells would cause ohmic losses⁴⁷. Then, MFCs performance
342 fueled by commercial xylan from corncob was tested under the optimal conditions established
343 according to above experiments. As shown in Fig. 5b, when the concentrations of corncob
344 xylan increased from 0.5 g/L to 1 g/L, the P_{\max} boosted from $111.82 \pm 5.35 \mu\text{W}\cdot\text{cm}^{-2}$ (green
345 line) to $174.33 \pm 4.56 \mu\text{W}\cdot\text{cm}^{-2}$ (peach pink line). However, further increase in concentrations
346 of xylan resulted in 12.22% decrease in power density (blue line), probably due to the poor
347 solubility and high viscosities of commercial xylan prepared in buffer solution. The P_{\max} of
348 our MFC fueled by 1 g/L xylan is $174.33 \pm 4.56 \mu\text{W}\cdot\text{cm}^{-2}$, which is significantly higher than
349 those for xylan-fueled MFCs inoculated with activated sludge ($0.609 \mu\text{W}\cdot\text{cm}^{-2}$) or rumen
350 microorganisms ($40.5 \mu\text{W}\cdot\text{cm}^{-2}$)^{13,48}.

351 In order to investigate the release and transfer of electrons in bioelectrochemical system,
352 Faraday efficiency (η_F) was determined (Supplementary Fig. 14). The current peaked at 2.07
353 mA at the onset time and then declined over time. In a batch reaction of 35 h, the cumulative
354 electric charges generated from 50 mL of reaction solution were 58.34 C. The concentration
355 of product α -ketoglutarate determined by HPLC was 3.19 mM, convertible to the yield of
356 46.6%, suggesting that the same amount of D-xylose was consumed and corresponding to

357 61.58 C of electricity. In consideration of a conversion efficiency of 97% from NADH to
358 electrons determined in a previous study⁴⁹, the η_F value was calculated to be 97.7%
359 ($58.34 \div 61.58 \div 0.97 \times 100\%$).

360

361 **Long-term electricity generation of MFCs fueled by hemicellulose fractions of corncob**

362 As xylan is a predominant component of hemicellulose, we next examined the performance of
363 MFCs powered by real hemicellulose. Biomass corncob pretreated by heating in alkaline
364 solution after neutralizing was used as fuels for power generation⁵⁰. 1.06 g/L xylan from the
365 pretreated hydrolysates of corncob was fueled, in which D-xylose was not detectable by
366 HPLC. To supply constant fuels to MFC, the above pretreated hemicellulose was
367 supplemented once a day to roughly maintain the same level. Then we examined the
368 performance of the MFC using enzyme-engineered-bacterial-consortia-modified-bioanode. As
369 shown in Fig. 6, the P_{max} of enzyme-bacterial-consortia-bioanode based MFC was $162.73 \pm$
370 $3.69 \mu\text{W}\cdot\text{cm}^{-2}$ (Fig. 6, black line). The remarkable power output of the
371 enzyme-bacterial-consortia-bioanode based MFC is much excelled over microbial community
372 based MFC¹³, possibly because diverse biological properties of various microorganisms in
373 one system may result in the instability in bacterial community. In addition, the long-term
374 generation of electricity was also evaluated. The bacterial-consortia-bioanode based MFC
375 maintained more than 95% of the P_{max} after 6 days' operation. On the contrary, the poor
376 stability was observed in other biomass-based sugar-fed enzymatic fuel cells⁵¹. Besides, the
377 conversion of pretreated hemicellulose from corncob to α -ketoglutarate was also monitored
378 during 6 days. The yield of α -ketoglutarate was 44.3% during the 6 days' long-term electricity
379 generation of MFC fueled by the pretreated hydrolysates of corncob (Fig. 6, red line).

380 Moreover, the morphology of the bacterial-consortia-bioanode was observed by scanning
381 electron microscope (SEM). After generating power for 6 days, the *E. coli* consortia and
382 MWCNTs were still closely bound to the CC, while the *E. coli* were intact (Supplementary
383 Fig. 15). These results indicate that the cells survived and stayed stable on CC during 6 days'
384 operation. These results suggest that the capabilities of engineered bacterial consortia can
385 efficiently convert hemicellulose biomass into high-value products and electric power.

386

387 In summary, a synthetic pathway that can generate high value-added chemical of
388 α -ketoglutarate and 4 electrons from hemicellulose in a controllable manner was successfully
389 constructed by integrating six enzyme-displayed strains into a high-efficient bacterial
390 consortia through tuning the expressed enzyme molecules and adjusting ratios of consortia
391 members. The production of α -ketoglutarate with excellent yield of 0.47 g/g was realized
392 within 6 h by the enzyme-engineered bacterial consortia surface-displayed saccharification
393 and oxidation pathway of xylan, the most abundant hemicellulose type. Then a
394 two-compartment xylan/O₂ MFC was assembled using enzyme-bacterial consortia modified
395 bioanodes and a laccase-displayed strain modified biocathode, realizing the direct conversion
396 of biomass into electricity and α -ketoglutarate. The optimized MFC realized 46.6% (w/w)
397 yield of α -ketoglutarate, the highest OCV and the largest P_{max} . The Faraday efficiency was
398 97.7%. Furthermore, this MFC exhibited a considerable power output and long-term stability
399 towards real biomass samples. To the best of our knowledge, this is the first example to use
400 engineered bacteria consortia as biocatalyst for efficient utilization of hemicellulose,
401 representing an important step toward further improving conversion of biomass to high
402 value-added chemical and powerful electric energy. Based on these results, we envision that

403 controllably enzyme-engineered bacterial consortia would find a wide range of applications in
404 the fields of metabolic engineering, synthetic biology, enzyme engineering, bioenergy and
405 enzymatic electrosynthesis.

406

407 **Methods**

408 **Strains and chemicals**

409 All strains and plasmids used in this study are listed in Supplementary Table 1. The primers
410 used are listed in Supplementary Table 2. *E. coli* DH5 α was used for gene recombinant
411 manipulation and *E. coli* BL21 (DE3) $\Delta xyLAB$ was used as host to express recombinant
412 proteins. Strains of *E. coli* carrying recombinant plasmids were routinely grown in
413 Luria-Bertani (LB) medium (10 g/L tryptone, 10 g/L NaCl, 5 g/L yeast extract) at 37 °C and
414 200 rpm. Whenever necessary, antibiotic (kanamycin, 50 μ g/mL) was added. Taq DNA
415 Polymerase and all restriction endonucleases were purchased from Fermentas (St. Leon Rot,
416 Germany). Kits used for molecular cloning were obtained from Sparkjade Biotech Co., Ltd
417 (Qingdao, China). Corncob xylan to represent hemicellulose were purchased from Meryer Co.
418 Ltd (Shanghai, China). 4-nitrophenyl- β -D-xylopyranoside (PNPX), ABTS, AQDS, D-xylose,
419 L-arabinose, xylono-1,4-lactone, D-xylonic acid lithium salt and α -ketoglutarate were
420 purchased from Sigma-Aldrich (St. Louis, MO, USA). Platinum (Pt) wire, Ag/AgCl electrode
421 and Nafion 117 membrane (N117) were purchased from Incole Union Technology Co. Ltd
422 (Tianjin, China). Multi-walled carbon nanotubes (MWCNTs) were purchased from Macklin
423 Biochem Technology Co. Ltd (Shanghai, China). Corncob was obtained from Corn Research
424 Center of Qingdao Agriculture University. Other chemicals were purchased from Solarbio
425 Science & Technology Co., Ltd (Beijing, China).

426 **Plasmids construction**

427 **Construction of the knockout plasmids**

428 For genetic operations into the genome of *E. coli* BL21 (DE3), the pRE112 suicide vector was
429 utilized. To construct plasmids pRE112- Δ *xyLAB*, approximately 862 bp upstream and 857 bp
430 downstream fragments of the *xyIA* and *xyIB* genes were amplified using the upstream primers
431 *xyLAB-Up-F/R* and downstream primers *xyLAB-Down-F/R*, respectively, and inserted into the
432 Kpn I site of pRE112. The plasmid pRE112- Δ *xyLAB* were transferred from *E. coli* χ 7213 to *E.*
433 *coli* BL21(DE3) by conjugation. Suitable recombinants were identified by antibiotic
434 resistance screening and sucrose reverse screening. The resulting strain *E. coli*- Δ *xyLAB* was
435 identified by PCR via the primers *xyLAB-1-F/R*.

436 **Construction of anchoring motif expressing plasmid**

437 The gene encoding N-terminal ice nucleation protein originating from *Pseudomonas borealis*
438 was amplified from vector pTInaPbN-Xdh by PCR using primers INP-F/INP-R, and inserted
439 into the *Nco* I/*Nde* I site of pET-28a (+) to generate plasmid pYJ-00.

440 **Constructions of hemicellulose hydrolytic enzymes expressing plasmids**

441 The gene encoding TtGH8 from *Teredinibacter turnerae* (GenBank No. CP001614.2), SXA
442 from *Selenominas ruminantium* (GenBank No. WP_026766185) were codon-optimized for *E.*
443 *coli* and synthesized by BGI Co., Ltd (Shenzhen, China). To construct intracellular protein
444 expression vectors pYJ-01 and pYJ-02, TtGH8 and SXA encoding gene and corresponding
445 cloning vector gene were amplified from above cloning plasmids and pET-28a by PCR
446 method using primers pET-28a-F(TtGH8)/pET-28a-R(TtGH8) & TtGH8-1-F/TtGH8-1-R,
447 pET-28a-F (SXA)/pET-28a-R (SXA) & SXA-1-F/SXA-1-R, respectively, and using the

448 ClonExpress Ultra One Step Cloning Kit (Vazyme Biotechnology, Nanjing, China). To
449 construct intracellular protein expression vectors pYJ-03, pYJ-01 and pYJ-02 vectors were
450 used as PCR templates and pET-28a-TtGH8-F/pET-28a-TtGH8-R & SXA-2-F/SXA-2-R as
451 primers, and two amplified gene fragments were ligated by in-fusion method using the
452 ClonExpress Ultra One Step Cloning Kit. For the construction of plasmids overexpressing
453 enzymes displayed on cell surface, TtGH8 and SXA encoding gene and corresponding
454 cloning vector gene were amplified from above cloning plasmids and pYJ-00 by PCR using
455 primers pET-28a-INP-F (TtGH8)/pET-28a-INP-R (TtGH8) & TtGH8-2-F/TtGH8-2-R,
456 pET-28a-INP-F(SXA)/pET-28a-INP-R(SXA) & SXA-3-F/SXA-3-R, respectively, and using
457 the ClonExpress Ultra One Step Cloning Kit to generate pYJ-04 and pYJ-05. Plasmid pYJ-06
458 was constructed using pYJ-04 and pYJ-05 as PCR templates and
459 pET-28a-INP-TtGH8-F/pET-28a-INP-TtGH8-R & SXA-4-F/SXA-4-R as primers by fusion
460 PCR strategy.

461 **Construction of pentose oxidative enzymes expressing plasmids**

462 To construct intracellular protein expression vectors pYJ-07, pYJ-08, pYJ-09, pYJ-10 and
463 pYJ-11, the genes encoding XDH, XylC, XylD, XylX, KGSADH were amplified from the
464 genomic DNA of *Caulobacter crescentus* NA1000³⁵ and corresponding cloning vector gene
465 was amplified from pET-28a by PCR method using primers pET-28a-F
466 (XDH)/pET-28a-R(XDH) & XDH-1-F/XDH-1-R, pET-28a-F (XylC)/PET-28a-R (XylC) &
467 XylC-1-F/XylC-1-R, pET-28a-F(XylD)/pET-28a-R(XylD) & XylD-1-F/XylD-1-R,
468 pET-28a-F(XylX)/pET-28a-R(XylX) & XylX-1-F/XylX-1-R,
469 pET-28a-F(KGSADH)/pET-28a-R(KGSADH) & KGSADH-1-F/KGSADH-1-R, respectively,

470 and using the ClonExpress Ultra One Step Cloning Kit. To construct intracellular protein
 471 expression vectors pYJ-12, pYJ-09 and pYJ-11 vectors were used as templates and
 472 pET-28a-XylD-F/pET-28a-XylD-R & KGSADH-2-F/KGSADH-2-R as primers, and two
 473 amplified gene fragments were ligated by in-fusion method (the ClonExpress Ultra One Step
 474 Cloning Kit). For the construction of plasmids overexpressing enzymes displayed on cell
 475 surface, XDH, XylC, XylD, XylX, KGSADH encoding genes was amplified from above
 476 cloning plasmids and corresponding cloning vector gene was amplified from pYJ-00 by PCR
 477 method using primers pET-28a-INP-F(XDH)/pET-28a-INP-R(XDH) & XDH-2-F/XDH-2-R,
 478 pET-28a-INP-F(XylC)/pET-28a-INP-R(XylC) & XylC-2-F/XylC-2-R,
 479 pET-28a-INP-F(XylD)/pET-28a-INP-R(XylD) & XylD-2-F/XylD-2-R,
 480 pET-28a-INP-F(XylX)/pET-28a-INP-R(XylX) & XylX-2-F/XylX-2-R,
 481 pET-28a-INP-F(KGSADH)/pET-28a-INP-R(KGSADH) & KGSADH-2-F/KGSADH-2-R,
 482 respectively, and using the ClonExpress Ultra One Step Cloning Kit to generate plasmids
 483 pYJ-13, pYJ-14, pYJ-15, pYJ-16 and pYJ-17. Plasmid pYJ-18 was constructed using pYJ-15
 484 and pYJ-16 as PCR templates and pET-28a-INP-XylD-F(XylX)/pET-28a-INP-XylD-R(XylX)
 485 & XylX-3-F/XylX-3-R primers by fusion PCR strategy (ClonExpress Ultra One Step Cloning
 486 Kit). Plasmid pYJ-19 was constructed using pYJ-15 and pYJ-17 as PCR templates and
 487 pET-28a-INP-XylD-F(KGSADH)/pET-28a-INP-XylD-R(KGSADH) &
 488 KGSADH-3-F/KGSADH-3-R primers by fusion PCR strategy (ClonExpress Ultra One Step
 489 Cloning Kit). Plasmid pYJ-20 was constructed using pYJ-19 and pYJ-16 as PCR templates
 490 and pET-28a-INP-XylD-KGSADH-F/pET-28a-INP-XylD-KGSADH-R &
 491 XylX-4-F/XylX-4-R primers by fusion PCR strategy (ClonExpress Ultra One Step Cloning

492 Kit).

493 **Construction of lac-expressing plasmid**

494 For the construction of plasmids overexpressing lac- displayed on cell surface, the gene
495 encoding laccase from *Bacillus subtilis*⁵² was subcloned into pYJ-00 to generate pYJ-21 by
496 BGI Co., Ltd (Shenzhen, China).

497 **Purification of cytoplasmic enzymes**

498 Cells expressing seven intracellular enzymes, including TtGH8, SXA, TtGH8-SXA, XDH,
499 XylC, XylD, XylX, KGSADH and XylDK (strain TtGH8, SXA, TtGH8-SXA, XDH, XylC,
500 XylD, XylX, KGSADH and XylDK), were separately grown overnight in LB medium with
501 kanamycin, and induced with 0.5 mM IPTG when cells had reached an OD₆₀₀ of 0.6. After
502 overnight growth at 16 °C, cells were harvested by centrifugation, resuspended in 40 mL 50
503 mM Tris–HCl (pH 7.0) buffer, broken by ultrasonication and centrifuged at 12000 g for 40
504 min at 4 °C to remove cell debris and unbroken cells. The soluble extract was applied to a 5
505 mL Ni-NTA column that had been equilibrated with 50 mM Tris–HCl (pH 7.0). Then the
506 column was washed consecutively with resuspended buffer and several washing buffer (20
507 mM Tris–HCl pH 7.0, 300 mM NaCl, 1 mM β-mercaptoethanol) containing increasing
508 amounts of imidazole (10, 20, 30 and 50 mM). The bound protein was eluted with elution
509 buffer (20 mM Tris–HCl pH 7.0, 300 mM NaCl, 200 mM imidazole, 1 mM
510 β-mercaptoethanol). Protein dialysis was conducted in a buffer (10 mM Tris–HCl pH 7.0
511 containing 100 mM NaCl, 1 mM β-mercaptoethanol) at 4 °C. Protein purity was analyzed by
512 sodium dodecyl sulphate-polyacrylamide gel electrophoresis (SDS-PAGE), and protein
513 concentration was determined by Bradford assay.

514 **Cell-surface display of enzymes and cell-surface location analysis**

515 For displaying enzymes on cell surface of *E. coli*, recombinant strains were cultured in LB
516 medium to an OD₆₀₀ of 0.6, 0.5 mM of IPTG was used to induce protein expression. For
517 laccase, cells were further cultured overnight at 16 °C, collected by centrifugation and
518 incubated in a buffer of Tris-HCl (50 mM, pH 7.0). The other cells were further cultured at
519 30 °C overnight, which were collected by centrifugation and incubated in Tris-HCl buffer (50
520 mM, pH 7.0). To determine the successful display of enzymes on the cell surface, outer
521 membrane proteins of recombinant strains and negative control strain were isolated⁵³. The
522 outer membrane protein fractions of related strains were analyzed by 10% (wt/vol)
523 SDS-PAGE.

524 For Western-Blot assay, samples were transferred to PVDF membranes at 100 mA for 10 min.
525 Anti-6×HisTag mouse monoclonal antibody (catalog number D191001, Sangon
526 Biotechnology, Shanghai, China) at 1:1000 was added and incubated for 3 h at room
527 temperature, then rinsed three times with phosphate buffered saline (PBS) with 0.05%(v/v)
528 Tween-20 (PBST). It was then incubated with goat anti-mouse immunoglobulin G
529 (IgG)-horseradish peroxidase (HRP) conjugate (catalog number D110068, Sangon
530 Biotechnology, Shanghai, China) for 1 h at room temperature, washed three times with PBST
531 and then once with PBS. The conjugation of antigen and antibody was detected with W-TMB
532 chromogenic kit (Sangon Biotechnology, Shanghai, China).

533 For Quantitative Immunoassay, outer membrane proteins of recombinant strains were
534 transferred to low fluorescent background PVDF membranes. Anti-6×HisTag mouse
535 monoclonal antibody at 1:1000 was added and incubated for 3 h at room temperature, then

536 rinsed three times with PBST. It was then incubated with goat anti-mouse IRDye 800CW
537 fluorescent secondary antibodies (catalog number 926-32210, LI-COR, Inc., Lincoln, NE) for
538 1 h at room temperature, and then washed with PBST, air dried, wrapped in aluminum foil,
539 and stored at 4 °C. LI-COR Odyssey CLx imaging system was used to detect bands on
540 membrane. The standard curve from known concentrations of purified recombinant XDH run
541 on the same blot was obtained. Specific protein bands are quantified by fluorescent signals
542 (excitation wavelength, 785 nm; emission wavelength, 820 nm) and a linear regression
543 equation generated from recombinant XDH to estimate concentrations of proteins.

544 For fluorescence imaging, the induced cells were washed with PBS and blocked in PBS
545 buffer containing 1% bovine serum protein (BSA) for 30 min at room temperature. Next
546 anti-6xHis tag mouse monoclonal antibody was added (1:100) after blocking, incubated
547 overnight at 4 °C, and incubated for 1 h the next day at room temperature. After three washes
548 with PBS, the cells were incubated with FITC-conjugated Donkey anti-Mouse IgG (1:100) for
549 2 h at room temperature. The cells after PBS washing were observed with Laser Scanning
550 Confocal Microscope (TCSsp5 II 03040101, Agilent, USA).

551 **Enzymatic activity assay**

552 Enzymatic activity was monitored by measuring the optical density at 600 nm (OD_{600}) for
553 cells using a Cary-60 UV-VIS spectrophotometer (Agilent Technologies, Inc., Santa Clara,
554 CA). Soluble commercial corncob xylan was prepared by water dissolution. TtGH8 activity
555 was assessed on 1 g/L soluble commercial corncob xylan in 50 mM Tris-HCl buffer pH 7.0
556 with 10 mM $CaCl_2$ at 37 °C. The reducing sugars released by TtGH8 hydrolysis reaction was
557 measured by DNS method with xylose as standard⁵⁴. SXA enzymatic activity was detected

558 using pNPX as the substrate at 37 °C. The product *p*-nitrophenol shows typical peak at 405
559 nm, which can be monitored by a spectrophotometer²⁶. Enzymatic activity of XDH was
560 assayed by detecting the generation of NADH at 340 nm and 37 °C using 10 mM D-xylose as
561 substrate as well as 1 mM NAD⁺ as coenzyme. For XylC, it can accelerate the hydrolysis of
562 xylono-1,4-lactone into D-xylonic acid to generate D-xylonic acid, which can reduce the
563 absorbance at 405 nm of *p*-nitrophenol. Enzyme activity was quantified by measuring the
564 decrease in the absorbance at 405 nm⁵⁵. Spontaneous hydrolysis of xylono-1,4-lactone was
565 analyzed without catalysts. Enzymatic activity of XylD was assayed according to a modified
566 procedure. In a typical assay, the reaction cocktail contained a certain amount of purified or
567 cells and D-xylonic acid. After incubation at 37 °C for a certain period, the samples were
568 mixed with solution containing 1% semi-carbazide hydrochloride and 1.5% sodium acetate.
569 Finally after incubation at 30 °C for 10 min, the 2-keto-3-deoxyxylic acid produced was
570 quantified by detection of the absorbance at 250 nm typical of semicarbazone³⁷. Enzymatic
571 activity of XylX was assayed spectrophotometrically in a coupled assay with the
572 corresponding previous dehydratase XylD and KGSADH.^{37, 56} The assay was performed in 50
573 mM Tris-HCl buffer (pH 7.0) with 10 mM MgCl₂ containing 20 mM D-xylonic acid and 1
574 mM NAD⁺. After the addition of purified enzymes or enzyme-surface displayed strains, the
575 mixture was incubated at 37 °C. The increasing absorbance at 340 nm caused by NADH
576 produced in the reaction was monitored. Glutaraldehyde was used as the substitute substrate
577 to measure the activity of KGSADH by following the rate of NAD⁺ reduction by measuring
578 the optical density at 340 nm⁵⁷. To determine kinetic constants of cell surface-displayed
579 enzymes, different amounts substrate was used to initiate a series of enzymatic assays. The

580 data were applied to the Michaelis-Menten kinetic model using Graph-Pad Prism 5 software
581 (www.graphpad.com). To determine the optimum pH for the *E. coli*-Lac, all enzymatic
582 activities of the whole-cell catalyst were measured by adding ABTS to the final concentration
583 of 5 mM at 37 °C by varying the pH values of the buffer solution (50 mM), including HAc–
584 NaAc buffer (pH 3–5.5), Na₂HPO₄–NaH₂PO₄ buffer (pH 6) and Tris–HCl buffer (pH 7–9).
585 The oxidation activity of *E. coli*-Lac towards ABTS was calibrated by measuring the
586 absorbance of the supernatant at 420 nm ($\epsilon=36 \text{ mM}^{-1}\text{cm}^{-1}$, referred to ABTS concentration).

587 **Optimization of protein induced expression conditions**

588 Recombinant strains were cultured in LB liquid medium at 37 °C and 200 rpm. To optimize
589 inducer concentration for overexpressing INP-fused proteins, IPTG at different concentrations
590 of 0.1 mM, 0.5 mM, 1 mM and 1.5 mM were used when cells grew to an OD₆₀₀ value of 0.6.
591 Protein expression was induced overnight, and the activities of whole cell catalyst were
592 determined as above described. In order to investigate the effects of induction temperatures on
593 intracellular and displayed proteins, 0.5 mM of IPTG were added in to cultures when cells
594 grew to an OD₆₀₀ value of 0.6. Protein expression was induced overnight at different
595 temperatures of 16 °C, 25 °C, 30 °C and 37 °C, and the activities of crude extract or whole
596 cell catalyst was determined as above described.

597 **Bioproduction of α -ketoglutarate**

598 Recombinant strains were cultured in LB medium to an OD₆₀₀ of 0.6, 0.5 mM of IPTG was
599 used to induce protein expression. Cells were further cultured at 30 °C overnight, which were
600 collected by centrifugation and incubated in Tris–HCl buffer (50 mM, pH 7.0). To produce
601 α -ketoglutarate, 100 mL of 50 mM Tris–HCl buffer (pH 7.0) with 10 mM MgCl₂, 10 mM

602 CaCl₂, 1.0 g/L commercial corncob xylan and 4 mM NAD⁺ were incubated with artificial
603 bacterial consortia (OD₆₀₀=10) in a flask, which was shaken in an incubator at 150 rpm and
604 37 °C for 6 h. The produced α-ketoglutarate was determined by HPLC.

605 **Preparation of bioanode and biocathode**

606 The thickness of CC (CeTech, Taiwan, China) is 0.32 ± 0.02 mm, which was cut into pieces
607 of 1.5×1.5 cm² and washed by sonication in water and anhydrous ethanol, respectively. A 100
608 μL of poly (acrylic acid)-MWCNTs dispersion (0.089 mg/cm²) was cast and dried in air to
609 acquire modified CC/MWCNTs. For the preparation of bioanode, 100 μL of the prepared cells
610 (OD₆₀₀=5.0) were dropped onto the CC/MWCNTs and dried at room temperature to obtain
611 CC/MWCNTs/cells modified electrodes. Then 50 μL of Nafion solution (0.1 wt%) was
612 syringed to the electrode surface to cover the electrode. For the modification of biocathode,
613 100 μL *E. coli*-Lac aqueous dispersion (OD₆₀₀=10.0) was coated on the CC/MWCNTs, and
614 subsequently, 50 μL of Nafion solution (0.1 wt%) was dropped onto the surface of the
615 resulting electrode, then dried at room temperature. The thus-prepared electrode was denoted
616 as CC/MWCNTs/*E.coli*-Lac. The onset potential is defined as the potential at which the
617 current or current density goes above 1 μA·cm⁻².

618 **Fabrication of MFC**

619 The dual-chamber hemicellulose/O₂ MFC was assembled with anodic compartment
620 containing the artificial bacterial consortia modified CC/MWCNTs/cells and cathodic
621 compartment containing CC/MWCNTs/*E.coli*-Lac, separated by a Nafion 117 proton
622 exchange membrane (DuPont, USA) with a diameter of 1.6 cm. The anodic electrolyte
623 consisted of 100 mM Tris–HCl buffer (pH 7.0) containing 100 mM NaCl, 10 mM MgCl₂, 10

624 mM CaCl₂, 4 mM NAD⁺ and xylan. 10 mM AQDS was used as mediator when necessary.
625 The cathodic electrolyte consisted of 100 mM Na₂HPO₄-citric acid buffer (pH 5.0) containing
626 0.5 mM ABTS. Polarization curves were obtained by performing linear sweep voltammetry
627 (LSV) at the scan rate of 1 mV s⁻¹ and 37 °C. The specific current (I) was recorded in real
628 time. The voltage (V) between the anode and the cathode was set as the Y-axis of polarization
629 curves. The output power (P) was derived via the relationship: P = V × I. The specific current
630 and power were normalized to the geometric area of the anode (1.5 cm × 1.5 cm = 2.25 cm²)
631 to obtain the current density and power density, respectively. The calculations of current
632 density and power density refer to Eq.(1) and Eq.(2), respectively:

$$633 \quad j_{\max} = I/2.25 \quad (1)$$

$$634 \quad P_{\max} = V \times I/2.25 \quad (2)$$

635 **Faradaic efficiency (η_F) assay**

636 The η_F was determined through amperometry at 0.45 V. The generation of current was
637 monitored during a reaction time in a volume of 50 mL at 37 °C. The reaction system
638 composed of 100 mM NaCl, 10 mM MgCl₂, 10 mM CaCl₂ and 4 mM NAD⁺, 1 g/L
639 commercial corncob xylan in 100 mM Tris-HCl buffer (pH 7.0). The production of
640 α -ketoglutarate was detected by HPLC. The total charge (C) was calculated according to the
641 generated current during the whole time. The η_F was calculated using the equation as
642 follows⁵⁸:

$$643 \quad \eta_F = \int I \times dt / (C_{\alpha\text{-KG}} \times V \times n \times F) \quad (3)$$

644 where I is the current generated, dt is the time to produce current, C _{α -KG} is the concentration of
645 produced α -ketoglutarate during the whole time, V is the reaction volume, n is the number of

646 electrons generated per D-xylose consumed, and F is Faraday constant=96,485 C per mole
647 electron.

648 **Long-term electricity generation of MFCs powered by pretreated hemicellulose**

649 To obtain the hemicellulose from lignocellulose, biomass sample corncob was pretreated⁵⁰.
650 The milled corncob was pretreated by 2.5 M NaOH with a solid to liquid ratio of 1:30 (g/mL)
651 at 115 °C for 1 h. After filtration, the filtrate was neutralized with 1 M acetic acid for use. The
652 amounts of xylan were determined by gradient precipitation with ethanol and then freeze
653 drying⁶. This pretreated hemicellulose was used as fuels to power MFC for monitoring
654 electricity and α -ketoglutarate generation. 100 μ L of the prepared cells (OD₆₀₀=10.0) was
655 dropped onto the 2 mg/mL of MWCNTs coated CC surface (2.25 cm²) and dried at room
656 temperature. The pretreated corncob was supplemented into anodic electrolyte daily to
657 maintain the constant concentration according to that of α -ketoglutarate. LSV was performed
658 every 12 h incubating at 37 °C during 6 days. The produced α -ketoglutarate was determined
659 by HPLC.

660 **Morphology observation of the bio-nanocomposite modified CC**

661 To determine whether the *E. coli* consortia and MWCNT were successfully attached to the
662 CC surface, scanning electron microscopic images of the modified CC were recorded using
663 JSM-7500F scanning electron microscopy (JEOL, Tokyo, Japan). The CC was first washed
664 three times with PBS, soaked with 2.5% glutaraldehyde, and fixed at 4 °C for 12 h. Next, the
665 fixed CC was cleaned three times with PBS for 5 min each time. Then the cleaned CC was
666 dehydrated with 30%, 50%, 70%, 90% and 100% ethanol for 5 min each time. Then the
667 dehydrated CC was further dehydrated with 30%, 50%, 70%, 90%, 100% tert-butanol/ethanol

668 for 5 min each time. After dehydration, the CC was frozen at -20 °C. Next, the frozen CC was
669 put into the freeze-drying machine (Songyuan Huaxing Biotechnology Co., Ltd, Beijing,
670 China) for freeze-drying. Then, the CC was pasted to the copper platform with conductive
671 glue, followed by gold spraying.

672 **Analytical methods**

673 Cell growth was monitored by measuring the optical density at 600 nm (OD₆₀₀) for cells using
674 a Cary-60 UV-VIS spectrophotometer. Concentrations of D-xylose, L-arabinose,
675 α -ketoglutarate were detected via Ultimate 3000 HPLC (ThermoFisher, USA) using an
676 Aminex HPX87H column. The mobile phase was 0.05 M H₂SO₄, and the flow rate was 0.6
677 mL min⁻¹ at a refractive-index detector at 50 °C⁵⁹. Cyclic voltammetry (CV) was performed
678 in a three-electrode configuration with CC/MWCNTs/cells as working electrode, an Ag/AgCl
679 reference electrode and Pt wire as auxiliary electrode connecting to a CHI 1000C potentiostat
680 (CH Instrument, Shanghai, China). The electrochemical reactions were performed at 37 °C.

681

682 **Statistics and reproducibility**

683 Statistical analyses were mainly performed using Microsoft Excel software (version 2021).
684 Double-tailed t test or one-way ANOVA and a posteriori test were used for variance analysis.
685 The data were expressed as mean \pm standard deviation (SD). Each group included at least
686 three independent biological samples. Compared to a reference sample, significance was
687 established with a *P*-value less than 0.05. No statistical method was used to predetermine
688 sample size. No data were excluded from the analyses. The experiments were not randomized.
689 The investigators were not blinded to allocation during experiments and outcome assessment.

690

691 **Data availability**

692 Data supporting the findings of this work are available within the paper and Supplementary
693 Information files. A reporting summary for this Article is available as a Supplementary
694 Information file. Source data are provided with this paper.

695

696 **References**

- 697 1. Schulte LA, et al. Meeting global challenges with regenerative agriculture producing food and
698 energy. *Nat. Sustain.* **5**, 384-388 (2022).
699
- 700 2. Qiao J, Sheng YJ, Wang MH, Li AN, Li XJ, Huang H. Evolving robust and interpretable enzymes
701 for the bioethanol industry. *Angew. Chem. Int. Edit.* **62**, e202300320 (2023).
702
- 703 3. Chen Z, et al. Exploitation of lignocellulosic-based biomass biorefinery: A critical review of
704 renewable bioresource, sustainability and economic views. *Biotechnol. Adv.* **69**, 108265
705 (2023).
706
- 707 4. Yuan JS, Pavlovich MJ, Ragauskas AJ, Han B. Biotechnology for a sustainable future: biomass
708 and beyond. *Trends Biotechnol.* **40**, 1395-1398 (2022).
709
- 710 5. Lynd LR, et al. Toward low-cost biological and hybrid biological/catalytic conversion of
711 cellulosic biomass to fuels. *Energ. Environ. Sci.* **15**, 938-990 (2022).
712
- 713 6. Li H, et al. Effect of structural characteristics of corncob hemicelluloses fractionated by
714 graded ethanol precipitation on furfural production. *Carbohydr. Polym.* **136**, 203-209 (2016).
715
- 716 7. Choi JW, Jeon EJ, Jeong KJ. Recent advances in engineering *Corynebacterium glutamicum* for
717 utilization of hemicellulosic biomass. *Curr. Opin. Biotechnol.* **57**, 17-24 (2019).
718
- 719 8. Xiao M, Liu Y-J, Bayer EA, Kosugi A, Cui Q, Feng Y. Cellulosomal hemicellulases: indispensable
720 players for ensuring effective lignocellulose bioconversion. *Green Carbon*, (2024).
721
- 722 9. Vuong TV, Master ER. Enzymatic upgrading of heteroxylans for added-value chemicals and
723 polymers. *Curr. Opin. Biotech.* **73**, 51-60 (2022).
724
- 725 10. Saha BC. Hemicellulose bioconversion. *J. Ind. Microbiol. Biotechnol.* **30**, 279-291 (2003).
726

- 727 11. Mahapatra DM, Mishra P, Thakur S, Singh L. Leveraging artificial intelligence in
728 bioelectrochemical systems. *Trends Biotechnol.* **40**, 535-538 (2022).
729
- 730 12. Xiao X, et al. Tackling the challenges of enzymatic (bio)fuel cells. *Chem. Rev.* **119**, 9509-9558
731 (2019).
732
- 733 13. Tao MN, et al. Enhanced denitrification and power generation of municipal wastewater
734 treatment plants (WWTPs) effluents with biomass in microbial fuel cell coupled with
735 constructed wetland. *Sci. Total Environ.* **709**, 136159 (2020).
736
- 737 14. Liu ZD, et al. Performance and microbial community of carbon nanotube fixed-bed microbial
738 fuel cell continuously fed with hydrothermal liquefied cornstalk biomass. *Nat. Commun.* **185**,
739 294-301 (2015).
740
- 741 15. Wu SK, Snajdrova R, Moore JC, Baldenius K, Bornscheuer UT. Biocatalysis: enzymatic synthesis
742 for industrial applications. *Angew. Chem. Int. Edit.* **60**, 88-119 (2021).
743
- 744 16. Cai M, Liu Z, Zhao Z, Wu H, Xu M, Rao Z. Microbial production of L-methionine and its
745 precursors using systems metabolic engineering. *Biotechnol. Adv.* **69**, 108260 (2023).
746
- 747 17. Fang SQ, et al. Controllable display of sequential enzymes on yeast surface with enhanced
748 biocatalytic activity toward efficient enzymatic biofuel cells. *J. Am. Chem. Soc.* **142**,
749 3222-3230 (2020).
750
- 751 18. Hasunuma T, Kondo A. Development of yeast cell factories for consolidated bioprocessing of
752 lignocellulose to bioethanol through cell surface engineering. *Biotechnol. Adv.* **30**, 1207-1218
753 (2012).
754
- 755 19. Fishilevich S, Amir L, Fridman Y, Aharoni A, Alfonta L. Surface display of redox enzymes in
756 microbial fuel cells. *J. Am. Chem. Soc.* **131**, 12052-12053 (2009).
757
- 758 20. Van Bloois E, Winter RT, Kolmar H, Fraaije MW. Decorating microbes: surface display of
759 proteins on *Escherichia coli*. *Trends Biotechnol.* **29**, 79-86 (2011).
760
- 761 21. Liu Z, et al. Combined cell-surface display- and secretion-based strategies for production of
762 cellulosic ethanol with *Saccharomyces cerevisiae*. *Biotechnol Biofuels.*, **8**: 162.
763
- 764 22. Naidu DS, Hlangothi SP, John MJ. Bio-based products from xylan: A review. *Carbohydr. Polym.*
765 **179**, 28-41 (2018).
766
- 767 23. Fowler CA, et al. Structure and function of a glycoside hydrolase family 8 endoxylanase from
768 *Teredinibacter turnerae*. *Acta Crystallogr. D.* **74**, 946-955 (2018).
769
- 770 24. Jordan DB, Li XL, Dunlap CA, Whitehead TR, Cotta MA. Beta-D-xylosidase from *Selenomonas*

- 771 *ruminantium* of glycoside hydrolase family 43. *Appl. Biochem. Biotechnol.* **137-140**, 93-104
772 (2007).
- 773
- 774 25. Jordan DB, Braker JD. Beta-D-xylosidase from *Selenomonas ruminantium*: thermodynamics of
775 enzyme-catalyzed and noncatalyzed reactions. *Appl. Biochem. Biotechnol.* **155**, 330-346
776 (2009).
- 777
- 778 26. Jordan DB, Braker JD. beta-D-Xylosidase from *Selenomonas ruminantium*: role of glutamate
779 186 in catalysis revealed by site-directed mutagenesis, alternate substrates, and active-site
780 inhibitor. *Appl. Biochem. Biotechnol.* **161**, 395-410 (2010).
- 781
- 782 27. Rodriguez GM, Hussain MS, Gambill L, Gao D, Yaguchi A, Blenner M. Engineering xylose
783 utilization in *Yarrowia lipolytica* by understanding its cryptic xylose pathway. *Biotechnol*
784 *Biofuels* **9**, 149 (2016).
- 785
- 786 28. Anandharaj M, et al. Constructing a yeast to express the largest cellulosome complex on the
787 cell surface. *Proc. Natl. Acad. Sci. U. S. A.* **117**, 2385-2394 (2020).
- 788
- 789 29. Liang B, Li L, Mascin M, Liu A. Construction of xylose dehydrogenase displayed on the surface
790 of bacteria using ice nucleation protein for sensitive D-xylose detection. *Anal. Chem.* **84**,
791 275-282 (2012).
- 792
- 793 30. Li L, Kang DG, Cha HJ. Functional display of foreign protein on surface of *Escherichia coli* using
794 N-terminal domain of ice nucleation protein. *Biotechnol. Bioeng.* **85**, 214-221 (2004).
- 795
- 796 31. Li HL, et al. The hydrolytic efficiency and synergistic action of recombinant xylan-degrading
797 enzymes on xylan isolated from sugarcane bagasse. *Carbohydr. Polym.* **175**, 199-206 (2017).
- 798
- 799 32. Zheng Z, Chen T, Zhao M, Wang Z, Zhao X. Engineering *Escherichia coli* for succinate
800 production from hemicellulose via consolidated bioprocessing. *Microb. Cell Fact.* **11**, 37
801 (2012).
- 802
- 803 33. Li XW, Chen Y, Nielsen J. Harnessing xylose pathways for biofuels production. *Curr. Opin.*
804 *Biotech.* **57**, 56-65 (2019).
- 805
- 806 34. Rossoni L, et al. Engineering *Escherichia coli* to grow constitutively on D-xylose using the
807 carbon-efficient Weimberg pathway. *Microbiology* **164**, 287-298 (2018).
- 808
- 809 35. Stephens C, Christen B, Fuchs T, Sundaram V, Watanabe K, Jenal U. Genetic analysis of a novel
810 pathway for D-xylose metabolism in *Caulobacter crescentus*. *J. Bacteriol.* **189**, 2181-2185
811 (2007).
- 812
- 813 36. Liu M, Ding Y, Xian M, Zhao G. Metabolic engineering of a xylose pathway for biotechnological
814 production of glycolate in *Escherichia coli*. *Microb. Cell. Fact.* **17**, 51 (2018).

- 815
- 816 37. Tai YS, et al. Engineering nonphosphorylative metabolism to generate lignocellulose-derived
817 products. *Nat. Chem. Biol.* **12**, 247-253 (2016).
- 818
- 819 38. Sun L, et al. Current advance in biological production of short-chain organic acid. *Appl.*
820 *Microbiol. Biotechnol.* **104**, 9109-9124 (2020).
- 821
- 822 39. Zeng W, Zhang H, Xu S, Fang F, Zhou J. Biosynthesis of keto acids by fed-batch culture of
823 *Yarrowia lipolytica* WSH-Z06. *Bioresour. Technol.* **243**, 1037-1043 (2017).
- 824
- 825 40. Stottmeister U, Aurich A, Wilde H, Andersch J, Schmidt S, Sicker D. White biotechnology for
826 green chemistry: fermentative 2-oxocarboxylic acids as novel building blocks for subsequent
827 chemical syntheses. *J. Ind. Microbiol. Biotechnol.* **32**, 651-664 (2005).
- 828
- 829 41. Yovkova V, Otto C, Aurich A, Mauersberger S, Barth G. Engineering the α -ketoglutarate
830 overproduction from raw glycerol by overexpression of the genes encoding
831 NADP⁺-dependent isocitrate dehydrogenase and pyruvate carboxylase in *Yarrowia lipolytica*.
832 *Appl. Microbiol. Biotechnol.* **98**, 2003-2013 (2013).
- 833
- 834 42. Tenhaef N, et al. Microaerobic growth-decoupled production of alpha-ketoglutarate and
835 succinate from xylose in a one-pot process using *Corynebacterium glutamicum*. *Biotechnol. J.*
836 **16**, 2100043 (2021).
- 837
- 838 43. Liu A, Lang Q, Liang B, Shi J. Sensitive detection of maltose and glucose based on dual
839 enzyme-displayed bacteria electrochemical biosensor. *Biosens. Bioelectron.* **87**, 25-30 (2017).
- 840
- 841 44. Zhu H, Li Y. Turning light into electricity, biologically. *Green Carbon* **1**, 14-19 (2023).
- 842
- 843 45. Li F, et al. Engineering *Shewanella oneidensis* enables xylose-fed microbial fuel cell.
844 *Biotechnol. Biofuels* **10**, 196 (2017).
- 845
- 846 46. Ali R, Mittal G, Sultana S, Bhatnagar A. Ameliorative potential of alpha-ketoglutaric acid (AKG)
847 on acute lung injuries induced by ammonia inhalation in rats. *Exp. Lung Res.* **38**, 435-444
848 (2012).
- 849
- 850 47. Gal I, Schlesinger O, Amir L, Alfonta L. Yeast surface display of dehydrogenases in microbial
851 fuel-cells. *Bioelectrochemistry* **112**, 53-60 (2016).
- 852
- 853 48. Zang GL, et al. Direct electricity recovery from *Canna indica* by an air-cathode microbial fuel
854 cell inoculated with rumen microorganisms. *Environ. Sci. Technol.* **44**, 2715-2720 (2010).
- 855
- 856 49. Zhu Z, Kin Tam T, Sun F, You C, Percival Zhang YH. A high-energy-density sugar biobattery
857 based on a synthetic enzymatic pathway. *Nat. Commun.* **5**, 3026 (2014).
- 858

- 859 50. Oliveira EE, et al. Xylan from corn cobs, a promising polymer for drug delivery: production
860 and characterization. *Bioresour. Technol.* **101**, 5402-5406 (2010).
861
- 862 51. Shi P, Wu R, Wang J, Ma C, Li Z, Zhu Z. Biomass sugar-powered enzymatic fuel cells based on a
863 synthetic enzymatic pathway. *Bioelectrochemistry* **144**, 108008 (2022).
864
- 865 52. Durao P, et al. Proximal mutations at the type 1 copper site of CotA laccase: spectroscopic,
866 redox, kinetic and structural characterization of I494A and L386A mutants. *Biochem. J.* **412**,
867 339-346 (2008).
868
- 869 53. Liang B, Liu Y, Zhao Y, Xia T, Chen R, Yang J. Development of bacterial biosensor for sensitive
870 and selective detection of acetaldehyde. *Biosens Bioelectron* **193**, 113566 (2021).
871
- 872 54. Ontanon OM, et al. EcXyl43 beta-xylosidase: molecular modeling, activity on natural and
873 artificial substrates, and synergism with endoxylanases for lignocellulose deconstruction.
874 *Appl. Microbiol. Biot.* **102**, 6959-6971 (2018).
875
- 876 55. Sutter JM, Johnsen U, Schonheit P. Characterization of a pentonolactonase involved in
877 D-xylose and L-arabinose catabolism in the haloarchaeon *Haloferax volcanii*. *FEMS Microbiol*
878 *Lett* **364**, (2017).
879
- 880 56. Wasserstrom L, Portugal-Nunes D, Almqvist H, Sandstrom AG, Liden G, Gorwa-Grauslund MF.
881 Exploring D-xylose oxidation in *Saccharomyces cerevisiae* through the Weimberg pathway.
882 *AMB Express* **8**, 33 (2018).
883
- 884 57. Borgstrom C, et al. Identification of modifications procuring growth on xylose in recombinant
885 *Saccharomyces cerevisiae* strains carrying the Weimberg pathway. *Metab. Eng.* **55**, 1-11
886 (2019).
887
- 888 58. Zhu Z, Zhang YP. In vitro metabolic engineering of bioelectricity generation by the complete
889 oxidation of glucose. *Metab Eng* **39**, 110-116 (2017).
890
- 891 59. Tai YS, et al. Engineering nonphosphorylative metabolism to generate lignocellulose-derived
892 products. *Nat. Chem. Biol.* **12**, 247-253 (2016).
893
894

895 **Acknowledgments**

896 This work is financially supported by the National Key Research and Development Program
897 of China (2021YFA0910400, A.L.) and National Natural Science Foundation of China
898 (22278233, B.L.; 22378222, J.M.Y.).

899 **Author contributions**

900 B.L., S.C., A.H.L., and J.M.Y. conceived and coordinated the study. B.L., A.H.L., S.C. and
901 J.M.Y. wrote the article with input from all other co-authors. B.L., J.Y., C.F.M., and L.W.
902 constructed the engineered strains, tested enzymatic activity and MFCs. Y.R.Z. and Z.C.L.
903 performed electrochemical testing. J.Y. conducted SEM characterizations. L.Z. and J.L.
904 performed biomass pretreatment. B.L., J.Y., C.F.M., and L.W. analyzed the experimental data.
905 All authors contributed to the writing of the manuscript.

906

907 **Competing interests**

908 The authors declare no competing interest.

909

910

911

912

913

914

915

916

917

918

919

920

921 **Table 1 The production of α -ketoglutarate by microbial cell factories or *in vitro* one-pot**
 922 **reaction using different substrates.**

Organism	Substrate	Time (h)	Yield (g/g)	Reference
<i>Y. lipolytica</i> H355A (PYC1-IDP1)	glycerol	117	40%	41
<i>Y. lipolytica</i> WSH-Z06	glycerol	204	47%	39
<i>C. glutamicum</i> WMB2 _{evo}	xylose	90	0.55%	42
<i>E. coli</i> consortia	xylan	6	47%	this study

923

924

925

926

927

928

929

930

931

932

933

934

935

936

937

938

939 **Figure Legends**

940 **Fig. 1 The saccharification and oxidative pathway of xylan catalyzed by bacterial**
941 **surface displayed enzymes using N-terminal region of ice nuclear protein as anchoring**
942 **motif.** The final product is α -ketoglutarate. TtGH8, β -1,4 xylanase; SXA, β -D-xylosidase;
943 XDH, D-xylose dehydrogenase; XylC, xylonolactonase; XylD, xylonate dehydratase; XylX,
944 2-keto-3-deoxy-D-xylonate dehydratase; KGSADH, 2,5-dioxopentanoate dehydrogenase.

945 **Fig. 2 The optimization of ratios and constituents of engineered bacterial consortia. a**
946 Relative production of reducing sugars using corncob xylan (1g/L) as substrate catalyzed by
947 engineered bacterial consortia involving in the saccharification of xylan (up-stream pathway)
948 with different cell density ratios of *E. coli*-TtGH8 to *E. coli*-SXA. 1 mL of 50 mM Tris-HCl
949 buffer (pH 7.0) with 10 mM CaCl₂ and 1.0 g/L commercial corncob xylan were incubated
950 with artificial bacterial consortia (OD₆₀₀=10) at 37 °C (*n* = 3 biologically independent
951 experiments). The bacterial consortia with the ratio of 3:7 produced the highest level of
952 reducing sugars compared to those with other ratios. **b** Relative production of NADH
953 catalyzed by different bacterial consortia using D-xylonic acid as substrate. When different
954 fusion proteins of XylD-KGSADH, XylD-XylX and XylD-XylX-KGSADH were separately
955 displayed on cell surface, the resultant strains were named as *E. coli*-XylDK, *E. coli*-XylDX
956 and *E. coli*-XylDXX, respectively. The total OD₆₀₀ of these four systems were the same and
957 the cell density ratios of different strains were the same in one system. 1 mL of 50 mM Tris-
958 HCl buffer (pH 7.0) with 10 mM MgCl₂, 20 mM D-xylonic acid and 1 mM NAD⁺ were
959 incubated with artificial bacterial consortia (OD₆₀₀=10) at 37 °C (*n* = 3 biologically
960 independent experiments). Strain *E. coli*-XylDXX as the control. The bacterial consortia
961 system composed of *E. coli*-XylDK and *E. coli*-XylX produced the highest level of NADH
962 compared to those with other system. **c** Relative production of α -ketoglutarate catalyzed by

963 different bacterial consortia involving in oxidation of pentose monosaccharides (down-stream
964 pathway) with various cell density ratios among *E. coli*-XDH, *E. coli*-XylC, *E. coli*-XylDK
965 and *E. coli*-XylX using D-xylose as substrate. 1 mL of 50 mM Tris-HCl buffer (pH 7.0) with
966 10 mM MgCl₂, 10 mM D-xylose and 1 mM NAD⁺ were incubated with artificial bacterial
967 consortia (OD₆₀₀=10) at 37 °C (*n* = 3 biologically independent experiments). The bacterial
968 consortia with the ratio of 1:5:20:25 produced the highest level of α -ketoglutarate compared
969 to those with other ratios. **d** Relative production of α -ketoglutarate catalyzed by different
970 bacterial consortia with various cell density ratios of up-stream pathway to down-stream
971 using corncob xylan (1g/L) as substrate at 37 °C for 6 h. The up-stream pathway included *E.*
972 *coli*-TtGH8 and *E. coli*-SXA with the optimal ratio of 3:7. The down-stream pathway
973 included *E. coli*-XDH, *E. coli*-XylC, *E. coli*-XylDK and *E. coli*-XylX with the optimal ratio
974 of 1:5:20:25. The total OD₆₀₀=10 of the bacterial consortia was applied. *n* = 3 biologically
975 independent experiments. The bacterial consortia with the ratio of 3:7 produced the highest
976 level of α -ketoglutarate compared to those with other ratios. Data are presented as mean \pm SD.
977 The statistical significance is determined by a two-sided t test, and ***, **, * indicate
978 *P*<0.001, 0.01, and 0.05, respectively. Source data are provided as a Source Data file.

979 **Fig. 3 Schematic drawing of electron transfer route and catalytic reactions in the**
980 **proposed two-compartment xylan/O₂ MFC.** The system was composed of the
981 enzyme-engineered bacterial consortia based bioanode and *E. coli*-Lac based biocathode.

982 **Fig. 4 The integration of the enzyme-engineered bacterial consortia for generating**
983 **electricity in MFC. a** CVs of the CC/MWCNTs/*E.coli*-Lac biocathode in 100 mM
984 Na₂HPO₄-citric acid buffer (pH 5.0) under N₂-saturated atmosphere without ABTS (black
985 line), and in the presence of 0.5 mM ABTS under N₂-saturated (red line) and under
986 oxygen-saturated atmosphere (blue line). Scan rate: 10 mV s⁻¹. **b** CVs of CC in electrolyte

987 solution (black line); CC/bacterial consortia in electrolyte solution containing xylan (1 g/L)
988 and NAD^+ (4 mM) (red line); CC/MWCNTs/bacterial-consortia in electrolyte solution
989 containing xylan (1 g/L) and NAD^+ (4 mM) (blue line); CC/MWCNTs in electrolyte solution
990 containing AQDS (10 mM) (green line). CC/MWCNTs/bacterial-consortia in electrolyte
991 solution containing xylan (1 g/L), NAD^+ (4 mM) and AQDS (10 mM) (purple line). The
992 electrolyte solution is 100 mM Tris-HCl buffer (pH 7.0) containing 100 mM NaCl, 10 mM
993 MgCl_2 and 10 mM CaCl_2 . Scan rate: 10 mV s^{-1} . **c** Profiles of potential versus current density
994 (j). MFC consisting of CC/MWCNTs/bacterial-consortia bioanode and
995 CC/MWCNTs/*E.coli*-Lac cathode, which contain 10 mM of AQDS in the anodic chamber
996 (peach pink line). MFC consisting of CC/MWCNTs bioanode and CC/MWCNTs/*E.coli*-Lac
997 cathode, which contained bacterial consortia and 1 mM of AQDS in the anodic chamber (blue
998 line). MFC consisting of CC/MWCNTs/bacterial-consortia and CC/MWCNTs/*E.coli*-Lac
999 biocathode, which contained 1 mM of AQDS in the anodic chamber (light green line). **d**
1000 Profiles of power density dependent on different bioanodes, which are the same as c. Scan
1001 rate: 1 mV s^{-1} . Abbreviation: CC: carbon cloth. Source data are provided as a Source Data
1002 file.

1003 **Fig. 5 The optimization of MFC performance. a** Effect of loading amounts of bacterial
1004 consortia onto the CC/MWCNTs/bacterial-consortia bioanode on the power output. The
1005 bioanodes were prepared by dropping 100 μL of the prepared cells with different OD_{600}
1006 values onto the CC/MWCNTs and dried at room temperature. The xylan concentration is 1.0
1007 g/L. The amounts of bacterial consortia were 5 OD (blue line), 10 OD (pink line) and 20 OD
1008 (green line), respectively. **b** Effect of concentrations of commercial corn cob xylan on the

1009 power output. The bioanodes were prepared by dropping 100 μ L of the prepared cells with
1010 10.0 OD₆₀₀. The concentrations of commercial corncob xylan were 0.5 g/L (blue line), 1.0 g/L
1011 (pink line) and 2.0 g/L (green line), respectively. Abbreviation: CC: carbon cloth. Source data
1012 are provided as a Source Data file.

1013 **Fig. 6 Long-term operation stability of MFC fueled by hemicellulose fractions of**
1014 **corncob.** The time-dependent power density curve (black line) and α -ketoglutarate titers (red
1015 line) of enzyme-bacterial-consortia-modified-bioanode based MFC. Electrical outputs (power
1016 density) from engineered bacterial consortia were shown. The production of α -ketoglutarate
1017 in MFC was measured every 12 h during 6 days. LSV was recorded every 12 h during 6 days.
1018 The systems absence of pretreated hemicellulose from corncob were used as negative controls
1019 (blue line representing power density curve and green line representing α -ketoglutarate titers).
1020 $n = 3$ biologically independent experiments. Data are presented as mean \pm SD. Source data
1021 are provided as a Source Data file.

1022